ICSV14
Cairns • Australia
9-12 July, 2007
14th International Congress on Sound & Vibration

EFFECT OF BOUNDARY CONDITIONS AND SOURCE TRUNCATION IN THE PREDICTION OF FLOW-GENERATED SOUND

Paula Martinez-Lera[1], Julien Christophe[2], Christophe Schram[1] and Jerome Anthoine[2]

[1]LMS International
3001 Leuven, Belgium
[2]von Karman Institute for Fluid Dynamics
1640 Rhode-St-Genese, Belgium
paula.martinez@lms.be

Abstract

The influence of the finiteness of the source domain on the application of Curle's analogy for the computation of flow-generated sound is investigated in the present work. Two aspects are studied: the spurious source of sound induced by CFD boundary conditions in incompressible simulations and the error due to the truncation of the integration source domain. Two validation cases are investigated: a synthetic vortex street and the flow past a confined cylinder, both at low Mach number. The confined flow case presents specific difficulties, related to the presence of boundaries in the near-field of the quadrupolar sources and the existence of dipolar sources.

1. INTRODUCTION

The hybrid approach has its origins in the aeroacoustical analogy pioneered by Lighthill [1] in the 1950's, which originates from an exact manipulation of the flow motion equations:

$$\frac{\partial^2 \rho'}{\partial t^2} - c_0^2 \frac{\partial^2 \rho'}{\partial x_i^2} = \frac{\partial^2 T_{ij}}{\partial x_i \partial x_j} \tag{1}$$

where $T_{ij} = \rho v_i v_j + \left(p' - c_0^2 \rho'\right)\delta_{ij} + \sigma_{ij}$ is the so-called Lighthill's tensor and p' and ρ' represent the fluctuations of pressure and density with respect to the reference values p_0 and ρ_0 defining the uniform and steady propagation medium; c_0 is the speed of the sound in the fluid, and $\boldsymbol{v}$ is the velocity of the fluid. If the viscous term contribution can be neglected and the flow is considered incompressible and isentropic, Lighthill's tensor can be approximated as $T_{ij} \approx \rho_0 v_i v_j$.

The analogy is based on interpreting the right-hand side of Eq. (1) as a source of sound, which may be obtained through an incompressible and relatively inexpensive CFD computation at low Mach numbers. The acoustic field may then be computed in a subsequent step through solving a linear acoustic propagation equation. The computational efficiency and economy of this approach makes it very attractive for many problems of practical interest, where a computation of the fully compressible flow equations is still too expensive [2].

Curle's variant of Lighthill's analogy is a popular approach when solid boundaries are involved in the sound production mechanism. Starting from an integral solution of Lighthill's equation integrated by parts and for a steady wall surface, the following is obtained [3]:

$$\rho'(\mathbf{x},t) = \int_{-\infty}^{t}\int_{V} \frac{\partial^2 G_0}{\partial y_i \partial y_j} T_{ij}\, \mathrm{d}^3\mathbf{y}\,\mathrm{d}\tau - \int_{-\infty}^{t}\int_{S} p' \frac{\partial G_0}{\partial y_i} n_i\, \mathrm{d}^2\mathbf{y}\,\mathrm{d}\tau \tag{2}$$

where G_0 is the free field Green's function. The volume integral in Eq. (2) provides a quadrupolar field generated by the free turbulence; the surface integral over the solid boundaries in the problem represents a dipolar field generated by the interaction between the unsteady flow and these boundaries.

An aspect of concern in the application of Curle's analogy is the finiteness of the source domain. We distinguish two main issues: *i*) errors occur during the computation of the source field, due to the limitation of the physical domain at boundaries complemented by ad-hoc Boundary Conditions (BC); *ii*) even when the computational domain is large enough and complemented by suitable BCs, usually only a subset of this domain is retained for the generation of the equivalent sources and truncation errors may arise. It was previously shown that the integration of the quadrupolar acoustic field may be largely influenced by the truncation of the wake, even when the contribution of the wake itself to the acoustic field is negligible [4]. This work aims at providing a joint study of some of these effects and their correction techniques, focused on the common tools and software that are used by industry.

The outline of this paper is as follows: in Section 2, we study the performance of several BCs by measuring the distortion of the vorticity field; in Section 3, we analyze the effect of truncating the source integration domain and correction approaches; in Section 4, we show numerical results for a confined cylinder; finally, we gather some conclusions in Section 5.

2. EFFECT OF CFD OPEN BOUNDARY CONDITIONS

The influence of open boundary conditions in incompressible flow simulations is a known issue; boundary conditions that are widely used have been found to distort the vortices crossing them. In this work, we analyze the impact of some of these effects over the acoustic field predicted through the application of an acoustic analogy. The commercial solver FLUENT v6.3 is used in this study, with the following BCs at the outlet:

- Condition 1 : Zero normal gradient : $\frac{\partial u}{\partial n} = 0$ and $\frac{\partial v}{\partial n} = 0$
- Condition 2 : Zero constant pressure : $P = 0$
- Condition 3 : Zero Lagrangian pressure derivative : $\frac{DP}{Dt} = 0$
- Condition 4 : Sponge zone + zero constant pressure

The first condition uses a reference pressure which is fixed to zero in time (in this work, the reference pressure is fixed on the intersection between the inlet and the lower wall), the value of pressure in the whole computational domain being recovered using the velocity and its derivatives through momentum conservation. For the three last conditions, the pressure field is recovered from the pressure fixed at the outlet BC. The fourth proposed BC uses a sponge zone extending downstream of the computational domain of interest, involving a stretching of the grid in the longitudinal direction, in order to avoid numerical reflections at the outlet [5]. The grid stretching acts like a filter, i.e. the large coherent structures of the flow are dissipated, preventing fluctuations from reaching the outlet. At the end of this sponge zone is placed a zero constant pressure BC.

These four BCs have been tested on a two-dimensional benchmark case proposed by Schäfer and Turek [6]. A cylinder of diameter D centered at $(x,y) = (2D,2D)$ is placed inside a channel of height $H = 4.1D$. The length of the channel is $L = 22D$ in the x streamwise direction. On the walls of the duct, no-slip conditions are set. The inlet flow condition is a constant parabolic velocity profile; the Reynolds number is $Re=100$, based on the average velocity at the inlet $\bar{U}$ and on the cylinder diameter D. The Strouhal number related to the shedding frequency f is defined as $St=Df/\bar{U}$. All results presented are made dimensionless with the reference values D, ρ_0 and $\bar{U}$, where ρ_0 is the density of the fluid. A non-dimensional time scale t^* is defined, based on the time periodicity T and the initial time t_0^* corresponding to the maximum of the lift coefficient computed on the surface cylinder.

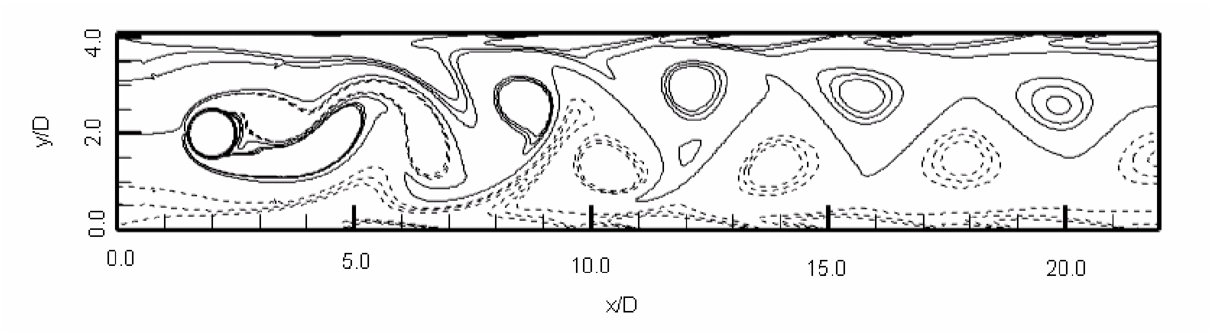

Figure 1 : Instantaneous flow vorticity contours for the sponge zone case. Contour levels are [0;±10;±12;±14] and negative values are dashed (t*=0).

The flow field was computed with the 2D unsteady laminar incompressible solver of FLUENT. The computational structured mesh contains 43680 hexahedral cells. In the sponge zone case, 2700 hexahedral cells were added. Around the cylinder and along the duct walls, the mesh is refined in order to capture correctly the boundary layer. Second order schemes are used for both space and time discretization. A time step of $\Delta t = 0.005D/\bar{U}$ is selected, yielding a CFL number below 0.5.

In Figure 1 instantaneous flow vorticity contours are plotted, showing the von Karman street formed by the fluctuating detachment of the boundary layer of the cylinder. The computed Strouhal number corresponding to the frequency of this detachment is $St = 0.30$. This value is in good agreement with the benchmark data predicting a value in the range $St = [0.2950;\ 0.3050]$. The maximum lift coefficient yields $C_{Lmax} = 1.04$ and the maximum drag coefficient is $C_{Dmax} = 3.28$; the benchmark bounds being respectively [$1.09;\ 1.01$] and [$3.22;\ 3.24$]. No significant variation of these parameters was observed due to the use of the different outlet BCs.

Figure 2 shows the behaviour of the different BC compared to the sponge zone case, for which the vortices leave the domain without visible distortion. As illustrated, the deformation of the vortices is limited to the neighbouring zone of the outlet BC, and is most visible near the duct walls. The distortion of the vorticity field for the zero normal gradient BC and the zero Lagrangian pressure derivative BC is negligible further than a length of $0.5D$ from the outlet. The zero pressure boundary condition induces a distortion over a somewhat larger part of the domain, but further from a distance D from the outlet the influence is negligible as well.

Figure 3 shows the relative error for the enstrophy in the domain compared to the sponge zone case for the different BCs. The enstrophy is defined as $\varepsilon = 1/2 \cdot \int \omega^2 dS$ and was integrated over the subdomain $x>3.5D$.

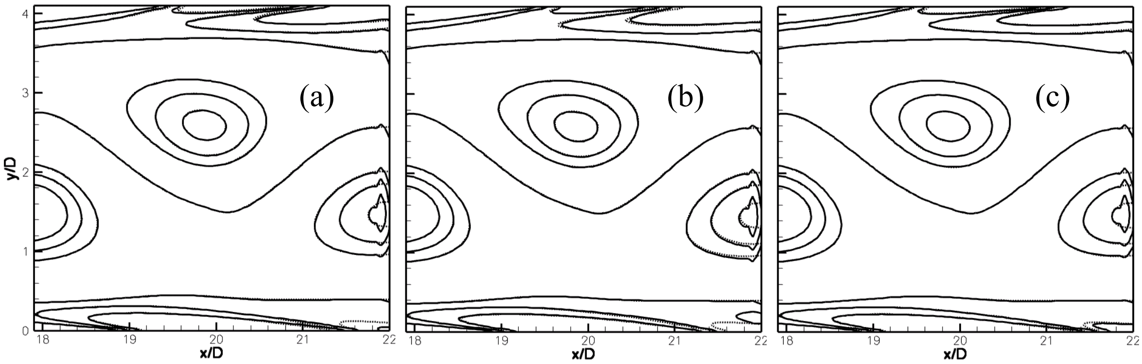

Figure 2 : Instantaneous flow vorticy contours for the zero normal gradient BC (a), the zero constant pressure BC (b); and the zero Lagrangian pressure derivative (c) compared to the sponge zone BC (dots). Contour levels are [0;±10;±12;±14]. t*=3/32.

As it can be observed, the zero pressure condition presents the largest error in terms of enstrophy conservation. By contrast, this comparison shows the improvement of a convective BC such as the zero Lagrangian pressure derivative BC, the error being the minimal for it. Similar trends where observed for the kinetic energy in the domain.

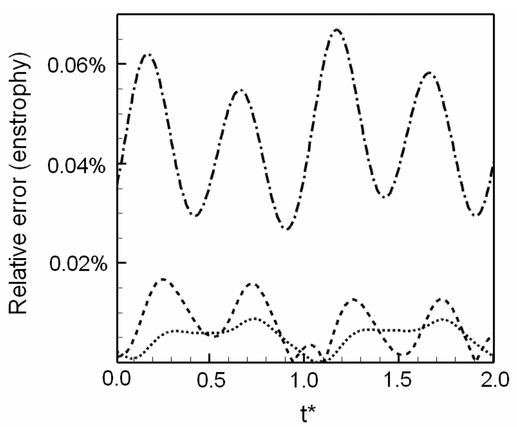

Figure 3 : Deviation of enstrophy from the sponge case for the zero normal gradient BC (dash), zero constant pressure BC (dash-dot), zero Lagrangian pressure derivative BC (dots). The error is defined as $|\varepsilon_b - \varepsilon| / \varepsilon_b$ (ε_b: enstrophy with sponge zone)

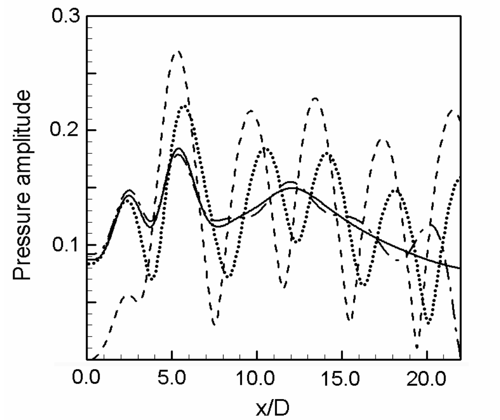

Figure 4. Amplitude of the pressure in Fourier domain for the lift frequency on the lower wall of the duct for the case: with sponge zone (solid), zero pressure BC (dash-dot), zero normal derivative (dash) and zero Lagrangian derivative (dots).

These results point at the conclusion that, whenever there is distortion of the acoustic quadrupolar source field due to the different BCs, these effects are restricted to a zone near the outlet, beyond which the error is negligible. This is not the case, however, for the pressure field, which has fundamental importance in Curle's analogy, as the dipole contribution is computed with the pressure on the walls. Figure 4 shows the amplitude of the Fourier transform of the pressure on the lower wall of the duct for the Strouhal frequency.

Far enough from the cylinder, the sponge zone case presents a smooth decay of the pressure towards the outlet. The zero pressure condition shows a somewhat deviated field, where some spurious fluctuations arise as a consequence of imposing a zero fluctuation at the outlet. The zero gradient condition presents by contrast large spurious fluctuations, in this case originated from the fact that the inlet is too close to the cylinder and thus the reference pressure is set on a point with significant pressure fluctuations. Moreover, the zero Lagrangian derivative condition also shows a strong deviation, due to the fluctuation of the levels of pressure in the domain due to the low reflectivity of the BC.

3. ERROR DUE TO THE TRUNCATION OF THE DOMAIN

The work by Wang et al. [4] illustrated the effect of truncation of the integration domain on the acoustic field for a case with an extensive wake, and proposed a correction term based on a frozen eddy assumption, relying on the fact that the wake is dominated by convection and thus basically silent at subsonic speeds. The correction involves the addition of a surface integral over the truncating surface Γ to the quadrupolar volume integral over the volume V of the domain of sources in Curle's analogy, leading to the quadrupolar field expressed in Fourier domain:

$$\hat{p}_{quadrup}(\mathbf{x},\omega) = \int_V \frac{\partial^2 \hat{G}_0}{\partial y_i \partial y_j} \hat{T}_{ij} \, \mathrm{d}^3\mathbf{y} - \int_\Gamma \frac{\partial^2 \hat{G}_0}{\partial y_i \partial y_j} \hat{T}_{ij} \frac{U_c}{i\omega} \mathrm{d}^2\mathbf{y} \tag{3}$$

The hatted variables are expressed in Fourier space; U_c stands for the convective velocity of the flow, and $i\omega$ is the imaginary unit times the angular frequency.

Other correction approaches, such as the use of a weighting function to make the sources decay close to the outlet [7], can be found in the literature. Both surface correction term and decaying functions approaches are tested and compared in this section.

3.1 Synthetic vortex street

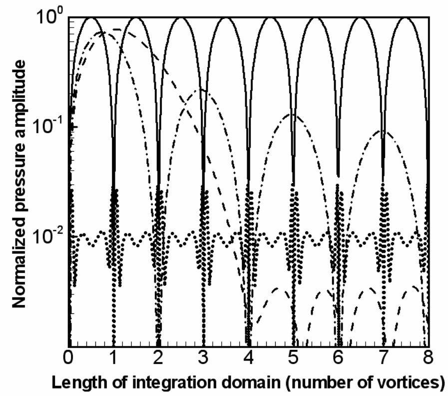

Figure 5. Normalized amplitude of acoustic field at a point vs. length of the integration domain. Uncorrected (solid line), corrected (dots), with linear weighting (dash-dot) and with Gaussian weighting with $\sigma_g/L = 0.3$ (dashed).

A synthetic velocity field of a vortex street was created by means of implementing a 2D row of Oseen vortices [8] that are convected along the x-axis. A row of 20000 vortices was implemented in order to mimic an infinite vortex street, whereas the integration domain comprised at most 8 vortices and was approximately centered in the middle of the row. As purely convected vorticity is silent at subsonic speeds, the acoustic field must yield zero.

The acoustic field was computed numerically. Figure 5 shows the evolution of the absolute value of the acoustic pressure at a monitoring point in the far field as the outlet limit of the domain is shifted from the inlet up to the total integration length of 8 vortices.

The figure shows the uncorrected acoustic pressure, as well as the acoustic pressure corrected through several means, namely, the correction term according to Equation (3), which was applied at the inlet and at the outlet, as well as two different weightings of the sources: linear and Gaussian weightings. The weighting functions are applied to the whole domain, taking a value one at the centre of the domain and decaying to zero at the inlet and outlet. All results have been normalized with the maximal value of the uncorrected pressure.

The uncorrected pressure shows a severe dependence on the size of the integration domain. The error reaches its minimum when the integration window extends over an integer number of hydrodynamic wavelengths. As it can be seen, the correction term succeeds to reduce very efficiently the error for any length of the domain, although a fluctuating error persists, which proved to be mainly due to sampling effects. Linear weighting is by contrast very inefficient, showing strong fluctuations that are only slowly reduced with an increasing domain length. The Gaussian function succeeds to decrease the error efficiently and with less sensitivity to numerical errors, but at the cost of a domain long enough to ensure a slow decay of the sources. With a long enough domain (around 4 vortices in the figure), only a small fluctuation remains. A small value of σ_g/L, with L being the length between the centre of the Gaussian function and the outlet, reduces this error further, but requires for it a larger domain; a good compromise was found for values of the variance around $\sigma_g^{\,2}=0.09\,L^2$.

3.2 Confined cylinder

In Figure 6 (upper row), directivity plots for the quadrupolar free field for several locations for the end of the integration domain are plotted. The CFD data were taken from the case computed with the sponge zone. The Mach number is $Ma=0.1$, based on the average inlet velocity U_{avg}. Velocity components inside the domain and pressure fluctuations on the walls are extracted in time during four periods and with 42 sampling intervals per period.

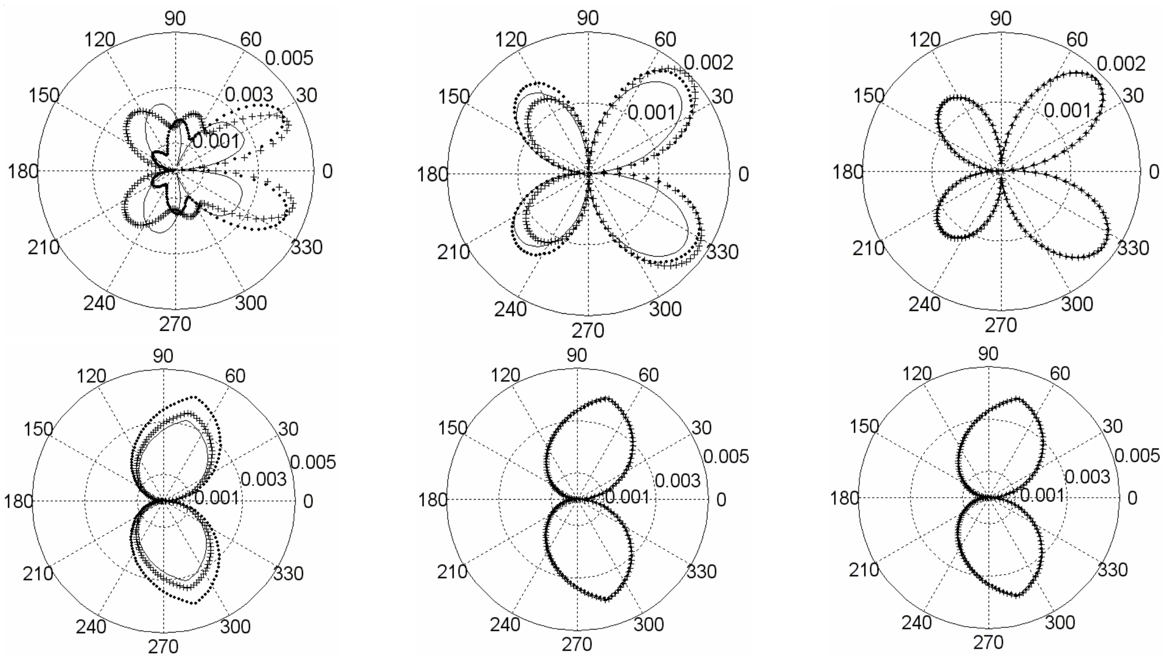

(a) (b) (c)

Figure 6. Directivity plot for the free quadrupolar field (*upper row*) and for the lower wall dipolar free field (*lower row*) at a distance $d=\lambda$ from the centre of the cylinder, for the lift frequency. In each figure, each line correspond to a different size of the integration domain, with the position of the integration outlet surface $x_{OUT}/D=18.5$ (solid line), *19.0* (+) and *19.5* (dots). ***(a)*** Uncorrected. ***(b)*** Corrected. ***(c)*** With Gaussian weighting.

As for the previous case, the criterion used for the assessment of the different correction methods is the independence of the sound prediction with respect to the extent of the source integration error, the convected von Karman street being merely dissipated by the action of viscosity and thus essentially silent. The results when no correction term is applied, as it can be seen, are largely dependant on the truncation location, making it unfeasible to compute with reasonable accuracy the acoustic field.

When the correction term is applied, the results present a fundamental improvement with respect to their independence from the downstream end location. The remaining variability may be attributed to the fact that inside a duct the pure convection hypothesis, on which the correction expression is based, is not accurate enough. The convection velocity which was used for this correction was $U_C=1.2\ U_{avg}$. Finally, the weighting of the sources with a Gaussian function gave the best results in terms of independence with respect to the downstream end location for this case.

In confined flows, the existence of non-compact dipolar sources creates an analogous problem to the quadrupolar field truncation. Indeed, the truncation of the dipolar sources on the walls may also induce an error. The correction term applied here is a direct extension of the correction term proposed in [4]. The justification for this is that the dipolar sources on the wall are correlated to the evolution of the velocity field in the domain, presenting similar evolution. These considerations allow deriving the following corrected dipolar field:

$$\hat{p}_{dipole}(\mathbf{x},\omega) = \int_S \frac{\partial \hat{G}_0}{\partial y_i}\,\hat{P}\,n_i \mathrm{d}^2\mathbf{y} - \int_\zeta \frac{\partial \hat{G}_0}{\partial y_i}\,\hat{P}\,n_i \frac{U_c}{i\omega}\,\mathrm{d}\mathbf{y} \tag{4}$$

In Equation (4), the correction term is an integral over the line ζ resulting from the intersection of the wall surface and the truncating surface. Figure 6 (lower row) shows directivity plots of the free field created by the dipolar sources in the lower wall of the duct. As it can be seen, both the correction term and the weighting approach succeed to increase the independence of the results from the downstream limit of the integration domain.

4. NUMERICAL BEM COMPUTATION

The acoustic field was computed numerically with the commercial software SYSNOISE Rev.5.6 through a boundary element method (BEM). A modified Curle's analogy proposed by Schram and Tournour [9], that takes into account the double nature of walls both as dipolar sources and as acoustic scattering entities, was applied.

The quadrupolar and dipolar sources which were inserted in the acoustic model were synthesized from the CFD computation where the sponge zone had been applied. The presence of the cylinder was modelled through a single equivalent dipole for each frequency, as it is compact. In order to correct the error due to the truncation of the CFD domain, a Gaussian weighting function centred in $x/D=7$ and with $\sigma=4.5D$ was applied to the quadrupoles in the part of the CFD domain comprised between $x/D=7D$ and $x/D=22D$, as well as to the dipole distribution on the walls of the duct.

A three-dimensional acoustic mesh was built for the BEM computation, with a relatively short spanwise length ($0.8D$), forcing a one-dimensional acoustic field for the frequencies of interest. The acoustic mesh extended beyond the CFD domain, namely from $x=-13D$ to $x=82D$, and contained 14928 elements distributed such that the mesh size was $\Delta x=0.2D$ inside the source region and $\Delta x=0.4D$ far from it. The mesh refinement near the source region is necessary in order to resolve properly the scattering of the quadrupoles over the walls of the duct. At the inlet and at the outlet mesh, a constant impedance $Z=\rho_0 c_0$ was prescribed as BC, making these ends anechoic for the considered frequencies, which are below the duct cut-off frequency. At the boundaries corresponding to the walls of the 2D duct, distributed wall dipoles coming from the CFD sources were applied in the part inside the source region.

Figure 7 shows the results of the acoustic pressure for a listener situated on a line parallel to the x-axis ranging from $lx=40D$ to $80D$, where lx is the distance to the centre of the cylinder. The results are compared to those obtained with a tailored Green's function for a 2D rectangular duct [10]. As it can be seen, for the lift frequency the deviation is significant. This is probably due to the fact that the inlet is too close to the cylinder in the CFD domain, such that a significant part of the dipolar sources on the wall is missing. Indeed, as it was shown in Figure 4, the fluctuation at the inlet for this frequency is still important; this comes to illustrate further the importance of the errors due to the truncation of the domain.

By contrast, the results for the drag frequency show an excellent agreement. In this case, the pressure fluctuation at the inlet is relatively small, so the error that arises for the lift coefficient is negligible in this case. These results confirm the capabilities of Curle's analogy in confined flows, and thus the relevance of the aspects related to the source treatment for its application that have been tackled in the present work.

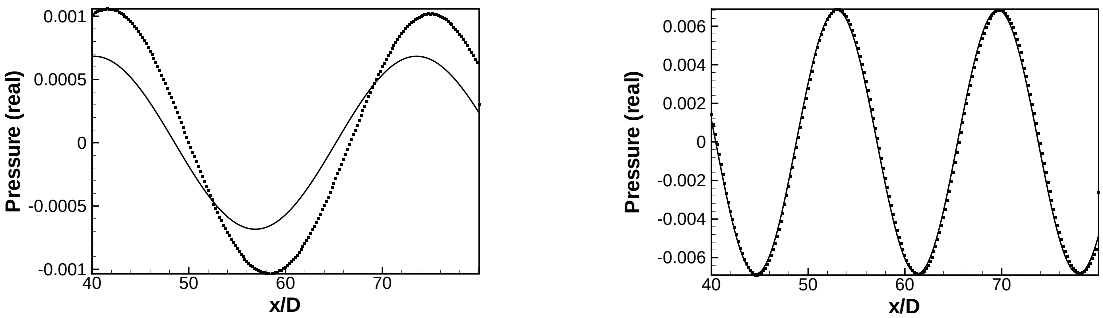

Figure 7. Acoustic pressure (real part) along the line *40D<lx<80D*, obtained through Curle's analogy computed numerically with BEM (dots) and through a tailored Green's function for a two-dimensional duct (solid line). *Left:* Lift frequency. *Right:* Drag frequency.

5. SUMMARY

The influence of CFD outflow boundary conditions on the application of Curle's analogy has been analysed through the confined flow past a cylinder inside a duct. Moreover, the effect of the finiteness of the quadrupolar source integration domain has been studied, and different correction approaches have been compared. The dipolar source truncation, as well as its correction, has been assessed by extension of the methods existing for the quadrupole sources. All these aspects are of relevance in the application of Curle's analogy.

The acoustic field for the confined cylinder case has been computed numerically with a Boundary Element Method. The results have been compared with those obtained with a tailored Green's function, showing the capabilities of Curle's analogy and the importance of a correct source treatment.

ACKNOWLEDGEMENTS

The authors gratefully acknowledge the EC support for the present work, performed within the Marie Curie EST project 'SIMVIA2' (www.simvia2.eu, contract nr MEST-CT-2005-020263).

REFERENCES

[1] M.J. Lighthill, "On sound generated aerodynamically. Part I. General theory", *Proceeding of the Royal Society of London* **A211**: 564-587 (1952)

[2] M. Wang, J.B. Freund and S.K. Lele, "Computational Prediction of Flow-Generated Sound", *Annual Review of Fluid Mechanics* **38**, 483–512, (2006)

[3] N. Curle, "The influence of solid boundaries upon aerodynamic sound", *Proceeding of the Royal Society of London,* **A23**: 505–514 (1955)

[4] M. Wang, S.K. Lele and P. Moin, "Computation of Quadrupole Noise Using Acoustic Analogy", *AIAA Journal* **34**, No.11, 2241–2254, (1996)

[5] T. Colonius, S.K. Lele and P. Moin, "Boundary conditions for direct computation of aerodynamic sound generation", *AIAA Journal* **31**, No.9, 1574-1582 (1993).

[6] M. Schäfer, S. Turek,: "Benchmark computations of laminar flow around cylinder", in E.H. Hirschel (editor), Flow Simulation with High-Performance Computers II, Vol. 52 ofNotes on Numerical Fluid Mechanics, 547-566, Vieweg, 1996

[7] A.A. Oberai, F. Roknaldin and T.JR. Hughes, "Computational procedures for determining structural-acoustic response due to hydrodynamic sources", *Comp. Methods Appl. Mech. Engrg.* **190**, 345-361, 2000

[8] P.G. Saffman, *Vortex Dynamics,* Cambridge Univ. Press, Cambridge, (1992)

[9] C. Schram and M. Tournour, "An innovative hybrid CFD/BEM method for the prediction of body-turbulence interaction noise", *Proceedings 13th International Congress on Sound and Vibration* (ICSV13), July 2–6 2006, Vienna, Austria

[10] P.M. Morse, K.U. Ingard, *Theoretical Acoustics,* McGraw-Hill Book Company, (1968)